ACS APPLIED MATERIALS & INTERFACES

Article

Hybrid Doping of Few-Layer Graphene via a Combination of Intercalation and Surface Doping

Ahmed E Mansour, Ahmad R. Kirmani, Stephen Barlow, Seth R. Marder, and Aram Amassian

ACS Appl. Mater. Interfaces, **Just Accepted Manuscript** • Publication Date (Web): 23 May 2017

Just Accepted

ACS Publications

ACS Applied Materials & Interfaces is published by the American Chemical Society.
1155 Sixteenth Street N.W., Washington, DC 20036

Hybrid Doping of Few-Layer Graphene via a Combination of Intercalation and Surface Doping

Ahmed E. Mansour[1], Ahmad R. Kirmani[1], Stephen Barlow[2], Seth R. Marder[2], Aram Amassian[1]*

[1]King Abdullah University of Science and Technology (KAUST), KAUST Solar Center (KSC), and, Division of Physical Science and Engineering (PSE), Thuwal, 23955-6900, Saudi Arabia

[2]Center for Organic Photonics & Electronics and School of Chemistry & Biochemistry, Georgia Institute of Technology, Atlanta, GA, 30332-0400, USA

*corresponding author: aram.amassian@kaust.edu.sa

KEYWORDS: Few-layer graphene, transparent conducting electrode, intercalation, molecular doping, work function, electrical transport

ABSTRACT: Surface molecular doping of graphene has been shown to modify its work function and increase its conductivity. However, the associated shifts in work function and increases in carrier concentration are highly coupled and limited by the surface coverage of dopant molecules on graphene. Here we show that few-layer graphene (FLG) can be doped using a hybrid approach, effectively combining surface doping by larger (metal-)organic molecules, while smaller molecules, such as Br_2 and $FeCl_3$, intercalate into the bulk. Intercalation tunes the carrier concentration more effectively, whereas surface doping of intercalated FLG can be used to tune its work function without reducing the carrier mobility. This multi-modal doping approach yields a very high carrier density and tunable increase in the work function for FLG, demonstrating a new versatile platform for fabricating graphene-based contacts for electronic, optoelectronic and photovoltaic applications.

Introduction

Graphene has been identified as a promising candidate material in optoelectronics, in photovoltaics and in emerging flexible and wearable electronic applications,[1–5] owing to its unique electronic,[6] optical,[7] and mechanical properties.[8] The linear electronic band structure[9] results in charge carriers behaving as massless Dirac fermions,[2,6] ambipolar field-effect transport,[10] and for extremely high quality graphene, ballistic transport,[11] and room-temperature carrier mobility values of ~200,000 $cm^2 V^{-1} s^{-1}$.[12] Moreover, single layer graphene absorbs only 2.3% of the visible light and thus exhibits high optical transmittance suitable for use as transparent conducting electrodes (TCE).[7,13] However, the intrinsic carrier density of high-quality pristine graphene sheets is low, typically on the order of ~10^9 cm^{-2},[11] and thus results in low electrical conductivity. Moreover, graphene is highly susceptible to environmental contaminants and impurities both on the top surface and the interface with the substrate, resulting in carrier-density-independent conductivity in the low-carrier-density regime.[14–16] Accordingly, methods to precisely control the quantity and type of charge carriers has been essential to enabling the use of graphene in various applications.[17,18] Moreover, if graphene is to be widely commercialized, large-scale production of graphene by chemical vapor deposition (CVD) is needed; this can either result in single-layer graphene (SLG) or few-layer graphene (FLG), depending on the transition metal used as catalyst.[19] The CVD process results in polycrystalline samples rife with grain boundaries and other defects which limit the electrical transport properties compared to what is achievable in high-quality mechanically exfoliated graphene;[20,21] thus, chemical doping is especially relevant to increasing the conductivity of FLG.[4,22]

Molecular surface doping of graphene has been demonstrated to be an effective route for work-function engineering in order to tune the energy barrier for extraction or injection of electrons at

graphene:semiconductor interfaces in devices.[23–26] For example tuning the work function of graphene is needed for applications as a low work function cathode or high work function anode in photovoltaics. Work-function modulation through surface doping occurs through the mutually reinforcing contributions of two mechanisms: (1) shift of the Fermi level (relative to the band positions of graphene) as a result of electron transfer to/from graphene for n- and p-doping, respectively, and (2) shift of the vacuum level due to the formation of surface dipole between the charged molecules and graphene.[27] Surface doping also leads to increased conductivity; however, this increase is limited by the often significant decrease in the carrier mobility due to Coulomb scattering by charged molecules (after electron transfer).[24,26,28,29] Graphene doping studies have mostly focused on SLG, in which the dopant molecules are present at the surface of graphene sheet, and where the carrier density can be increased up to values of ca. 10^{13} cm^{-2};[27,30] moreover, in some cases the exposed dopant ions present on the surface may be susceptible to degradation by environmental conditions.[31] Interlayer doping of graphene, in which SLG is sequentially transferred repeatedly onto a previously doped SLG, has been introduced to further increase the carrier density and enhance the stability of the dopants.[30–33] The interlayer doping process is repeated until the stack achieves the desired conductivity. However, this process is extremely cumbersome and potentially introduces defects and impurities in every transfer step; in addition some dopants may be incompatible with the transfer process.

FLG has emerged in recent years as a more resilient form of graphene exhibiting higher conductivity and performance stability under stretching and bending than SLG.[34–36] Moreover, FLG offers the opportunity for modulation of its electrical and electronic properties due to its ability to undergo intercalation reactions with molecular oxidants and reductants in a manner analogous to graphite, which has long been known to form graphite intercalation compounds

with small molecules.[37] This allows for effective doping of most, if not all, buried layers, depending on the staging of the intercalate molecules, thereby achieving carrier densities of up to 10^{15} cm^{-2},[38,39] a regime which is not accessible through the conventional molecular surface doping of either SLG or FLG. The encapsulation of dopant between the graphene sheets also potentially leads to higher stability of the doped material.[38–42]

The combination of large carrier density and work-function tunability in graphene would greatly increase its versatility to be used in electronic and optoelectronic applications; in principle this can be achieved through the combination of the two doping modalities described above – bulk intercalation and molecular surface doping – and their application to FLG. Here, we report the first results of such combination: CVD-grown FLG was p-doped through intercalation with either Br_2 or $FeCl_3$ followed by molecular-surface p-doping using tris(4-bromophenyl)ammoniumyl hexachloroantimonate, "Magic Blue", or molybdenum tris(1-(trifluoroacetyl)-2-(trifluoromethyl)ethane-1,2-dithiolene), "Mo-(tfd-$COCF_3$)$_3$" (both of which have previously been shown to be effective surface dopants for FLG).[43] Angle-resolved XPS data are presented that support the proposed structure of the doped FLG, in which the intercalants are primarily located within the bulk layers while the surface dopant are present on the topmost layer without any unfavorable mixing or chemical reactions. Systematic characterization of the electrical-transport properties shows that the enhancement of the conductivity is dominated by the increase of the carrier density from ~3×10^{13} cm^{-2} to ~6×10^{14} cm^{-2}. We show that the work function is further increased with surface doping of intercalated FLG while additionally improving the conductivity. The intercalation doping tunes the work function mainly by shifting the Fermi level, while the surface dopants provide further tunability by also shifting the vacuum level. Our approach leads to a ten-fold decrease of sheet resistance to

100 Ω/□ and a work function as high as 5.43 eV, corresponding to an increase of ca. 0.5 eV relative to pristine FLG. The hybrid doping approach of FLG demonstrated in the work provides an unmatched tunability of these figures of merit via careful selection of intercalant and surface dopants, and thus provides a promising and versatile route to modulate the properties of graphene for various electronic and optoelectronic applications.

Experimental methods

Sample preparation and doping: CVD-grown FLG (4 to 10 layers) on nickel (300 nm) on SiO_2/Si was purchased from the Graphene Supermarket and used as-is (more details are provided in the supplementary information). FLG was lifted-off and transferred to a glass substrate using the standard PMMA transfer procedure.[35] Our hybrid doping approach comprises two doping steps: (1) intercalation (bulk) doping; and (2) surface molecular doping. The intercalation process was carried out first to prevent potential chemical reactions between the potentially reactive intercalants and the surface dopants, and to avoid exposing surface dopants to the high-temperature process involved in the intercalation of $FeCl_3$. Washing the intercalated FLG prior to surface doping is a crucial step for removal of unreacted and weakly adsorbed intercalants from the surface of the FLG, so as to prevent unfavorable interactions with the molecular surface dopants. Two different intercalants were used: $FeCl_3$, which is capable of intercalating between every layer in FLG (stage 1); and Br_2, which intercalates between every two layers of graphene (stage 2).[37] Intercalation of FLG with $FeCl_3$ was carried out using a two-zone vapor-transport method, in which anhydrous $FeCl_3$ powder (800 mg) was placed downstream and heated at 320 °C and the FLG sample was placed upstream at 360 °C in a vacuum sealed tube. The process was carried out for 360 min, during which time the pressure reached ~ 5.6 mbar. Intercalated FLG was then rapidly cooled in air and subsequently washed under a flow of DI water for few

seconds in air and blown dry with N_2. Br_2 intercalation of FLG was carried out by exposure to bromine vapor at room temperature for 180 min in a glass enclosure placed inside a nitrogen-filled glove box. Brominated FLG was then washed under a flow of ethanol for few seconds in air and blown dry with N_2. Surface molecular p-doping of FLG was carried out using either tris(4-bromophenyl)ammoniumyl hexachloroantimonate "Magic Blue" (MB) or molybdenum tris(1-(trifluoroacetyl)-2-(trifluoromethyl)ethane-1,2-dithiolene) "Mo(tfd-$COCF_3)_3$ (Mo), which have redox potentials of +0.70 V and +0.39 V vs. ferrocenium/ferrocene ($FeCp_2^{+/0}$), respectively.[44,45] Solution doping was carried out by dipping the intercalated FLG in solutions (0.1 mg mL^{-1}) of either Magic Blue in dichloromethane or Mo(tfd-$COCF_3)_3$ dopant in toluene for 60 min inside a N_2 glove box. The samples were then washed inside the glovebox by the respective solvent used to apply the dopant so as to remove weakly bound species and blown dry with N_2. The various doping steps for obtaining hybrid-doped FLG, along with the expected location of the intercalant dopants and surface dopants, are illustrated in **Scheme 1**.

Characterization: Angle-resolved x-ray photoelectron spectroscopy (ARXPS) was used as a means for non-destructive depth profiling, to locate the position of the intercalants and surface dopants within the hybrid-doped FLG. The spectra were obtained using an Omicron Nanotechnology (Taunusstein, Germany) ultra-high vacuum (UHV) system. XPS was measured with a monochromatic Al Kα source (1486.7 eV). A hemispherical energy analyzer EIS-Sphera was used to collect the spectra with a pass energy of 40 eV for survey spectra and 20 eV for high-resolution spectra. A base pressure of about $< 5.0 \times 10^{-9}$ mbar was maintained throughout all measurements. The electron take-off angle – defined as the angle to the surface of the sample – was tuned by changing the orientation of the sample with respect to the detector, where the

surface sensitivity of the measured spectrum increases by decreasing the photoelectron take-off angle.

Raman spectra were obtained using a LabRAM ARAMIS (Horiba Jobin Yvon, Inc) instrument using a 473 nm laser excitation, focused with a 100× objective with a spot size of 1 μm and 0.5 mW power. The scattered signal was dispersed with using 1800 mm^{-1} grating. The spectra in the range from 1200 to 2900 cm^{-1} were collected in backscattering geometry.

Electrical transport measurements were performed using a linear 4-point probe (Jandel Engineering Ltd.) to deduce sheet resistance. In addition, room-temperature Hall effect measurements (Lake Shore 7700) were performed to deduce the carrier density and mobility of the samples, using the van der Pauw configuration with a reversible sweep of magnetic fields up to 20 kG using a 100 μA excitation current. Contacts were fabricated using conductive silver paste to fix low strain Ag alloy wires (Lake Shore PN 671-260), which were soldered to the sample holder.

Photoelectron spectroscopy in air (PESA) (Model AC-2, RKI instruments Inc.) was used to measure the work function. A tunable energy UV source was used, while the intensity fixed at 1000 nW.

Results and Discussion

Hybrid doping of the surface and bulk of few-layer graphene (FLG)

The hybrid doping approach combining the intercalation doping of FLG followed by surface molecular dopants is schematically illustrated in Scheme 1. Hybrid doping aims to maximize the doping efficiency and tunability of the properties of FLG through having the larger molecular dopants on the exposed graphene surface, while the smaller intercalant molecules occupying the

bulk of FLG, where they can dope all or some of the buried graphene layers, depending on the staging type of the intercalant molecules. The surface molecular dopant's interactions are expected to be largely confined to the surface of graphene, and thus, as desired, minimal interaction is expected with the intercalant molecules that are effectively encapsulated by the graphene layers. For this purpose, washing the intercalated FLG with appropriate solvents, depending on the choice of intercalant, as detailed in the experimental section, is crucial in order to remove the loosely bound species from the surface and allow more effective surface molecular doping of FLG samples.

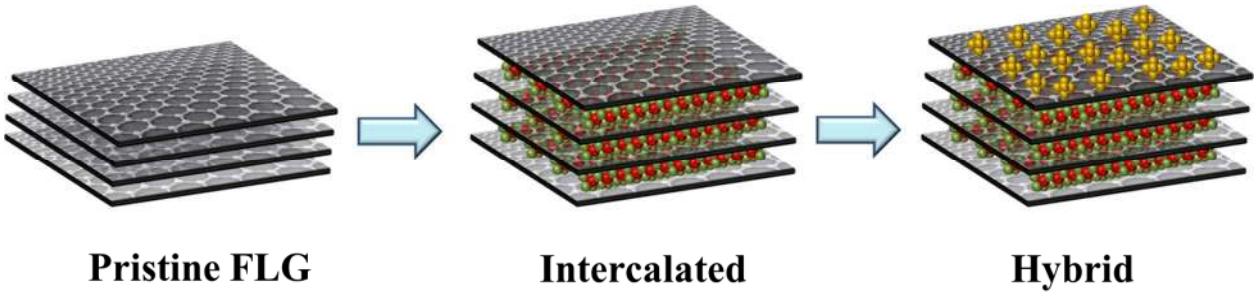

Scheme 1: FLG hybrid-doping approach, showing $FeCl_3$ intercalants encapsulated in between the graphene layers in FLG, while the $SbCl_6^-$ ions from the surface dopant Magic blue are exclusively present at the surface in hybrid doped FLG.

X-ray photoelectron spectroscopy (XPS) survey spectra of pristine, $FeCl_3$-intercalated, and hybrid-doped FLG with Magic blue (MB) as the surface dopant and $FeCl_3$ as intercalant (hybrid $FeCl_3$-MB) are shown in **Figure 1A**. The coexistence of both doping modalities in the sample is evident by the appearance of both Sb 4d (surface) and Fe 3p (intercalant) peaks in the hybrid doped sample as shown in the inset of **Figure 1A**. Similarly, the XPS survey spectra of Br_2-intercalated and Br_2-MB hybrid-doped FLG shown in **Figure 1B** indicates the coexistence of bromine intercalant (Br 3d) and antimony (Sb 4d) from the surface dopant (although the tris(4-bromophenyl)ammoniumyl cation of MB also contains Br, it is expected, and has been previously demonstrated in MB surface doping of FLG,[43] that the neutral tris(4-bromophenyl)amine side product of doping will be removed by

washing, leaving only the hexachloroantimonate anion on the surface). To confirm the spatial distribution of the two types of dopant ions, we tuned the surface sensitivity of XPS measurements by conducting ARXPS as shown in **Figure 1C** for hybrid $FeCl_3$-MB and **Figure 1D** for hybrid Br_2-MB. As XPS becomes more surface sensitive at small electron take-off angles, it detects the topmost graphene layers of the sample, where the molecular surface dopant ions reside. However, the entire depth of the FLG sample is detected at 90° electron take-off angle and thus the Sb/C atomic ratio is expected to be lower. Consistent with this expectation, the Sb/C atomic ratio gradually increases as the take-off angle is decreased from 90° to 20°, as shown in **Figures 1C and 1D** for both hybrid $FeCl_3$-MB and hybrid Br_2-MB, respectively. ARXPS reveals that the amount of $FeCl_3$ intercalant gradually decreases with increasing surface sensitivity, as indicated by the decrease of the Fe/C atomic ratio (**Figure 1C**), whereas the Br_2 intercalant is uniformly present inside FLG, as indicated by a nearly constant Br/C atomic content over all electron take-off angles. This points to the minimal presence of $FeCl_3$ on the surface of FLG and demonstrates the effectiveness of the washing step in removing the excess $FeCl_3$. The ARXPS data also indicate that intercalation of $FeCl_3$ is more concentrated toward the bottom of FLG and closer to the substrate, suggesting that a full stage 1 intercalation has not been achieved uniformly throughout the sample. We conducted control experiments on intercalated-only FLG and observed similar trends in the atomic ratio of Fe/C and Br/C for both $FeCl_3$ and Br_2 intercalated FLG, respectively (shown in Figure S2), to those seen in the respective hybrid-doped samples, indicating that the distribution of intercalated dopant species is inherent to the intercalation process, rather than being artifacts of the hybrid doping procedure. This is currently a limitation for the intercalation of CVD FLG due to intrinsic differences in crystallinity and interlayer coupling from HOPG.[46] Recent reports on $FeCl_3$-intercalated FLG have shown that

full intercalation could only be achieved for mechanically exfoliated FLG, the structure of which closely resembles that of graphite,[41,42,47] whereas in the case of CVD FLG, non-uniform and incomplete intercalation was found under the same processing conditions.[46] Overall, the XPS analysis confirms that the large molecular dopant is predominantly located on the surface, whereas the smaller intercalating dopant is primarily located in the bulk.

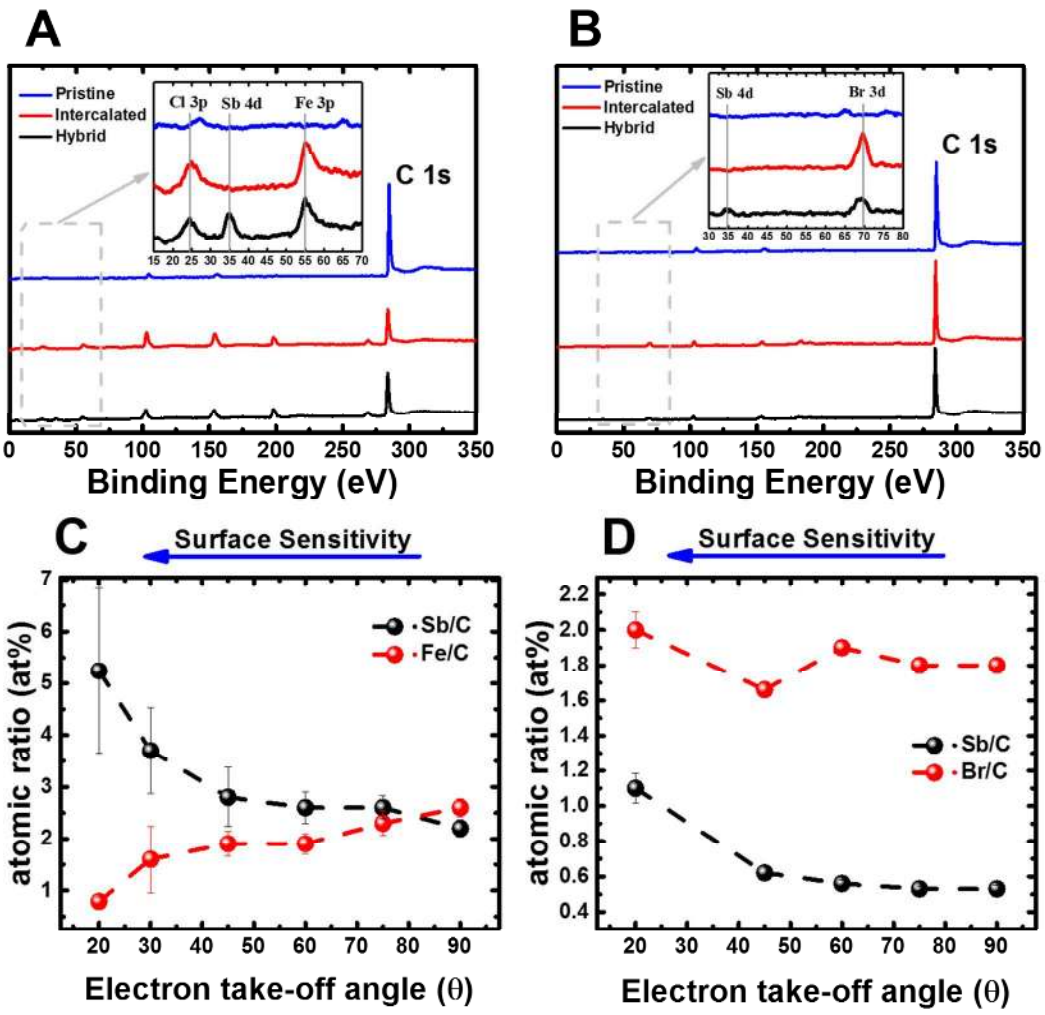

Figure 1: Survey XPS spectra showing the coexistence of bulk intercalants and surface dopants (A) pristine, $FeCl_3$ intercalated and hybrid $FeCl_3$-MB and (B) pristine, Br_2 intercalated and hybrid Br_2-MB. Angle-resolved XPS for (C) hybrid $FeCl_3$-MB, (D) hybrid Br_2-MB, The electron-take off angle (θ) shown on the x-axis determines the surface sensitivity of the measurement, where the smaller value indicates increasingly surface sensitive spectra as indicated by the blue arrow.

A comparison of the total amount of the surface dopant ($SbCl_6^-$ ions from Magic Blue) in the hybrid $FeCl_3$-MB and hybrid Br_2-MB FLG samples reveals that the former exhibits a larger Sb content of ~5 at%, while the latter exhibits a significantly smaller amount of ~1.1 at%. It is not clear why the intercalation process would impact the surface doping process. One possible explanation is that surface doping might be affected by the chemical modification of graphene, which is evident with Br_2 intercalation and less so with $FeCl_3$ intercalation.[48] Covalently bonded bromine atoms on the surface and step edges of FLG cannot be removed by the washing step as previously shown,[40] and may inhibit the surface dopant from interacting with FLG through an electron-transfer process. By contrast, the $FeCl_3$-intercalated sample does not show evidence of covalent bonding with carbon.[48,49] (more details are provided in the supplementary information)

Effects of intercalation and surface doping on Raman Spectra of FLG

Figure 2A shows Raman spectra of pristine and intercalated FLG with Br_2 and $FeCl_3$. The spectrum of pristine FLG shows the two main peaks characteristic of graphitic materials, namely, the G-peak at ~1580 cm^{-1}, resulting from the in-plane stretching mode (E_{2g}) originating from the optical phonon near the Γ point, and the second-order 2D-peak at ~2743 cm^{-1}, which arises from two optical phonons at the K point. The D-peak, which typically appears at ~1350 cm^{-1}, is activated by the presence of defects and exhibits very low intensity, highlighting the high quality of the graphene domains in our samples.[50] The 2D-peak could be fitted with two Lorentzian peaks, with the lower and higher energy components showing similar intensity. This is attributed to randomly rotated stacking and agrees with previous results on epitaxially grown FLG.[51] Upon exposure to the intercalants, the G-peak splits into a doublet, as shown in **Figure 2A**, with the lower energy peak positioned around that of the pristine FLG and originating from graphene layers not adjacent to intercalant, and a higher energy peak from intercalant-adjacent graphene

layers, the position of which is generally dependent on the staging, the degree of intercalation, and the doping strength of the intercalant.[37,42,52] Raman shifts in the low-energy G-peak position for pristine, intercalated, and hybrid-doped FLG are shown in **Figure 2B**, with the inset showing the high-energy G-peak shifts. Both G-peak components shift to successively higher energy with intercalation and with subsequent hybrid doping, these shifts being an established signature of doping in graphene.[53] It can be seen that the shift is larger in the case of $FeCl_3$ intercalation, consistent with a larger doping effect due to its ability to intercalate into every interlayer spacing in FLG (stage 1), as compared to Br_2 intercalation, which forms a stage 2 compound.[37] This is in agreement with XPS results indicating a higher atomic content of iron as compared to bromine (**Figure 1**) and with the larger decreases in the C 1s binding energies observed in the case of $FeCl_3$ intercalation (shown in **Figure S3).** The same trend is also observed for the low-energy fitted components of the 2D-peak shown in **Figure 2C**, which is more sensitive to the electronic structure and doping effects in FLG.[43] The additional shifts in the Raman peaks observed after surface doping of the intercalated FLG are in agreement with the XPS data in the case of $FeCl_3$ intercalation and consistent with the hybrid-doping approach contributing towards more efficient doping of all available layers in FLG. On the other hand, XPS data in the case of Br_2 intercalation do not show the additional shift in C 1s binding energy when subsequently surface doped; the reason for this is not clear, but is perhaps related to the above-mentioned covalent surface functionalization that occurs with this dopant (see below).

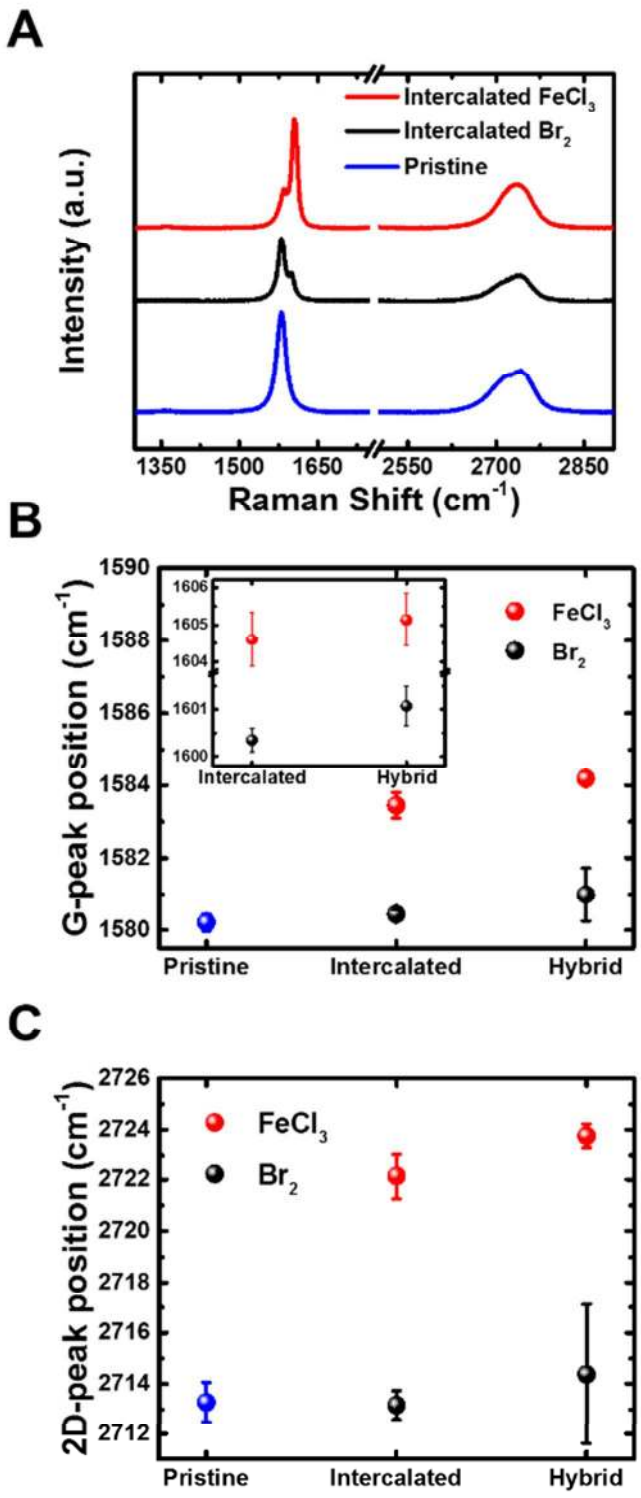

Figure2: (A) Raman spectra of pristine and intercalated FLG with either Br_2 or $FeCl_3$. Changes of the Raman shift of (B) the G-peak components and (C) the 2D-peak low energy component for intercalated and hybrid $FeCl_3$-MB and Br_2-MB doped FLG.

Transport properties of hybrid-doped FLG

The average sheet resistance of pristine FLG on glass is 860 Ω/□, as measured using a linear 4-point probe. Upon intercalation with Br_2 the sheet resistance decreases to 390 Ω/□, which is further reduced in hybrid Br_2-MB doped FLG to 240 Ω/□. A similar trend is observed for the hybrid $FeCl_3$-MB doped FLG, where $FeCl_3$ intercalation results in a sheet resistance reduction to 140 Ω/□, which further decreases with surface doping to 100 Ω/□, as shown in **Figure 3A**. The sheet resistance of FLG that is only surface doped with Magic Blue is approximately halved to 420 Ω/□, demonstrating that the combination of surface and intercalation doping of FLG is more effective for increasing electrical conductivity than either method alone. However, it seems that the choice of the surface dopant is important: using $Mo(tfd\text{-}COCF_3)_3$ (Mo) with $FeCl_3$-intercalated FLG (hybrid $FeCl_3$-Mo) resulted in a sheet resistance of 170 Ω/□, higher than obtained using intercalation alone.

The overall conductivity results from a balance between the injection of additional free charge carriers and the loss of carrier mobility due to Coulomb scattering. We further elucidate the effects of these doping modalities on the transport properties of FLG by conducting Hall effect measurements at the various steps leading up to hybrid doping of FLG. In **Figure 3B** we show the changes in the carrier density, which is found to increase significantly following $FeCl_3$ intercalation from 3.1×10^{13} cm^{-2} for pristine FLG to 4.8×10^{14} cm^{-2}, nearly an order of magnitude higher than surface doping with Magic Blue alone (8×10^{13} cm^{-2}). It is thus clear that intercalation of FLG results in effective doping of a significant number of the buried graphene layers as compared with surface doping. Intercalation of FLG with Br_2 has a more moderate effect than $FeCl_3$, resulting in a modest increase of the carrier density to 5.7×10^{13} cm^{-2}, consistent with the lower atomic content of bromine as compared with $FeCl_3$, as discussed earlier (Figure 1). For the

hybrid-doped FLG, the carrier density increases further to 5.9×10^{14} cm^{-2} in the case of hybrid $FeCl_3$-MB and to 8×10^{13} cm^{-2} in the case of hybrid Br_2-MB, indicating that the hybrid doping approach works well in both cases in terms of increasing the density of free carriers. In **Figure 3C** we compare the changes in the charge-carrier mobility for the various approaches. It is reduced significantly with intercalation, decreasing threefold from ~289 $cm^2V^{-1}s^{-1}$ for pristine FLG to 89 $cm^2V^{-1}s^{-1}$ for $FeCl_3$-intercalated FLG. Coulomb scattering is believed to be responsible for this, especially the presence of $FeCl_3$ between every graphene layer due to its lower staging. The scattering effect has been demonstrated to be comparatively low in FLG with surface doping, since the charged dopant molecules (after electron transfer) are screened by the buried graphene layers within FLG.[43] The mobility therefore decreases by 32% to ~196 $cm^2V^{-1}s^{-1}$ in the case of MB-doped FLG, as shown in **Figure 3C**. Interestingly, the addition of surface doping to intercalation of FLG in the hybrid $FeCl_3$-MB case does not seem to adversely affect the carrier mobility further, resulting in a mobility of 91 $cm^2V^{-1}s^{-1}$, which is effectively unchanged from, if not slightly higher than, that obtained using $FeCl_3$ intercalation alone, resulting in a net increase in the conductivity of the sample. The overall decrease of the charge-carrier mobility by 65% is thus more than compensated by a 1800% increase of the overall carrier density of the hybrid-doped $FeCl_3$-MB sample. Bromine intercalation causes a more moderate loss of carrier mobility, down to 255 $cm^2V^{-1}s^{-1}$, and surface doping further reduces the mobility moderately to a value of 220 $cm^2\ V^{-1}\ s^{-1}$. Nevertheless, hybrid Br_2-MB doping shows a smaller reduction in the carrier mobility as compared to surface doping alone, demonstrating the effectiveness of the hybrid-doping approach.

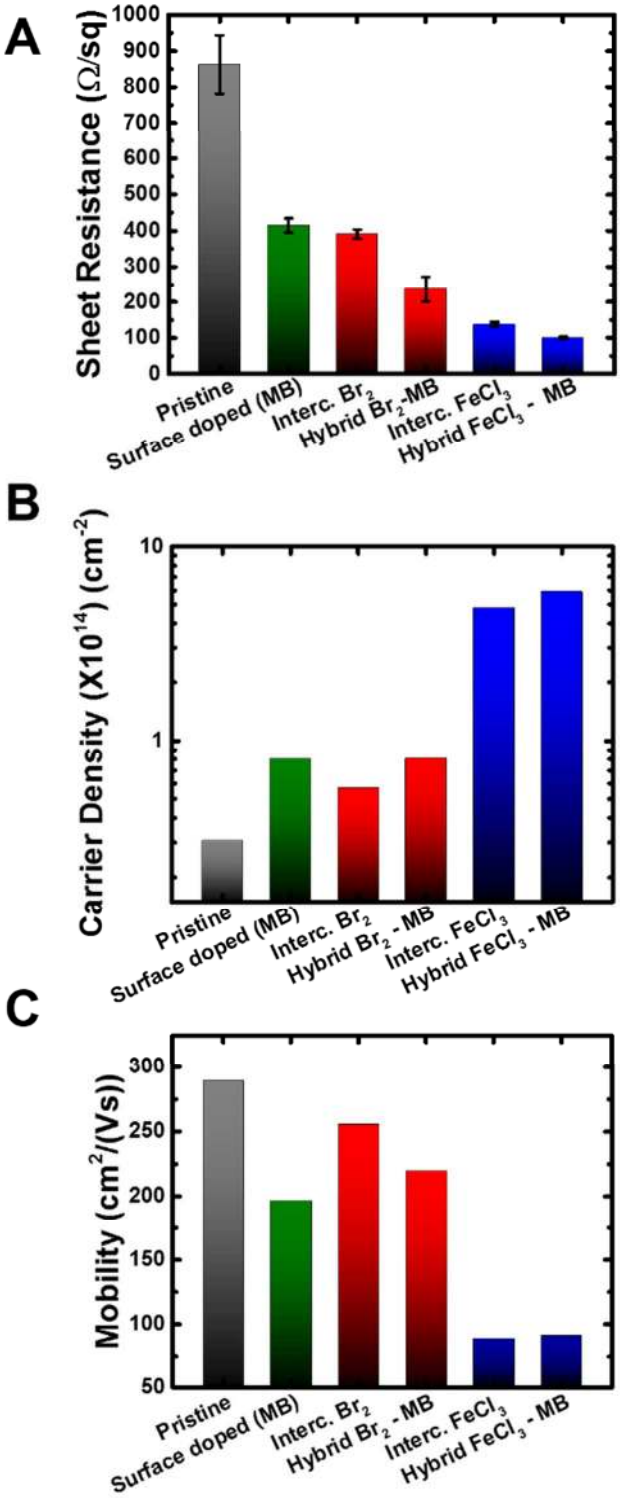

Figure 3: Electrical Transport properties. (A) Sheet resistance as measured by linear 4-points probe -error bars indicate the standard deviation of nine different spots on each sample-, (B)

Sheet carrier density and (C) and carrier mobility, for pristine, surface doped with magic blue, intercalated with either $FeCl_3$ or Br_2 and hybrid doped FLG.

Work function tunability

The effect of the various dopant modalities on the work function was evaluated by photoelectron spectroscopy in air (PESA) and is shown schematically in **Figure 4** (PESA spectra are shown in **Figure S5**). Pristine FLG exhibited a value of 4.88 eV. Upon intercalation, the work function increased by 0.20 eV to 5.08 eV for Br_2 intercalation and by 0.41 eV to 5.29 eV for $FeCl_3$ intercalation. The larger increase in the work function for the case of $FeCl_3$ intercalation as compared to Br_2 is consistent with XPS, which indicated a qualitatively larger shift in the Fermi energy level for the former intercalant, Raman, and Hall-effect measurements. Applying surface dopants to the intercalated FLG results in additional increase of the work function. The hybrid Br_2-MB sample work function increases by 0.19 eV beyond that of the intercalated FLG to 5.27 eV (total shift of 0.39 eV), whereas the work function of hybrid $FeCl_3$-MB increases by 0.14 eV to 5.43 eV (total shift of 0.55 eV).

Hybrid doping using $FeCl_3$ as the intercalant and $Mo(tfd\text{-}COCF_3)_3$, which has a less oxidizing redox potential than Magic Blue, as the surface dopant results in a more moderate increase of the work function (by 0.05 eV), highlighting the ability to more independently tune the work function than by surface doping alone, all the while achieving high conductivity enabled through intercalation.

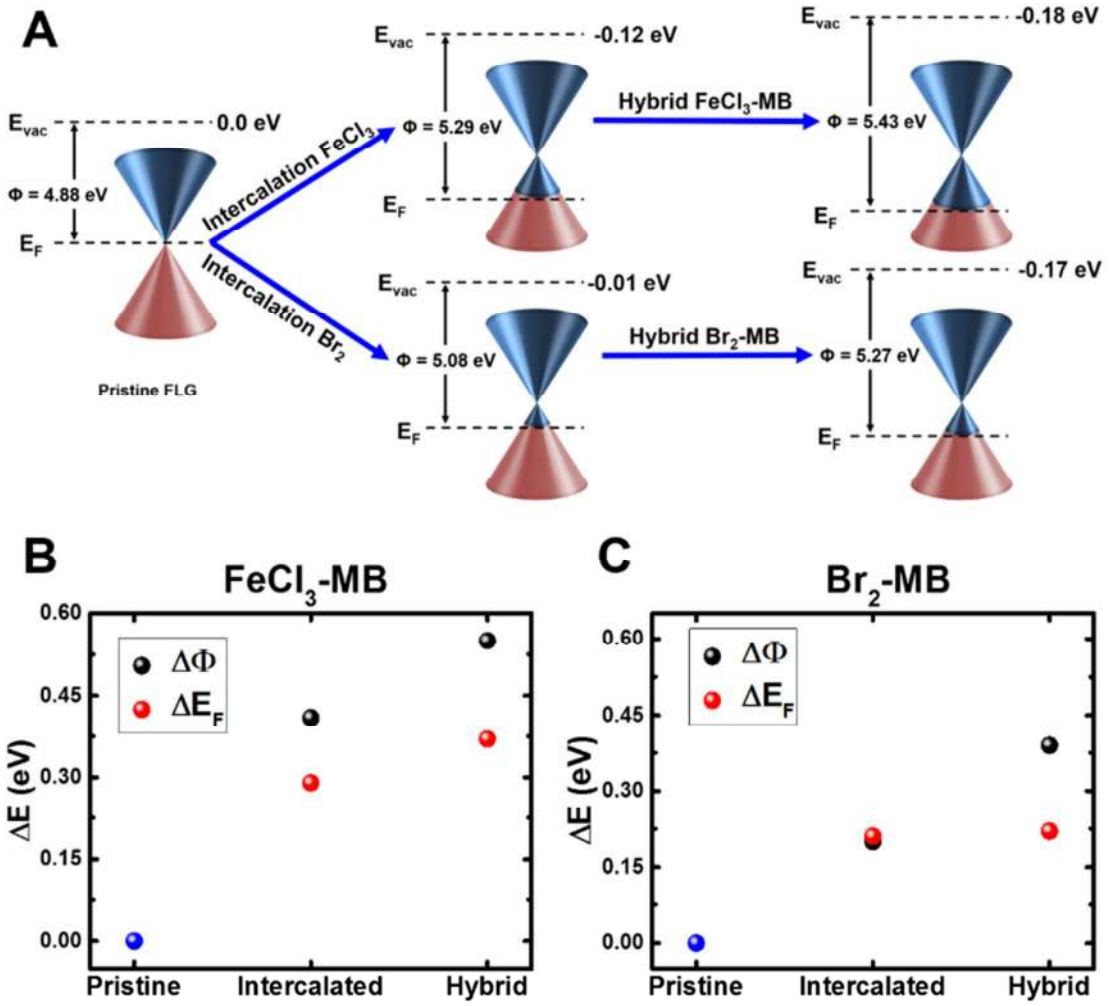

Figure 4: (A) Schematic representation of the work function of pristine FLG showing the Fermi level (E_F) coinciding with the Dirac cone, and the vacuum level (E_{vac}) at 0.0 eV, and their changes after intercalation with $FeCl_3$ and hybrid $FeCl_3$-MB doping (top) and after intercalation with Br_2 and hybrid Br_2-MB doping (bottom). Quantitative relative changes of the work function changes (PESA) and E_F changes (XPS C 1s peak) for (B) intercalated $FeCl_3$ and hybrid $FeCl_3$-MB and (C) intercalated Br_2 and hybrid Br_2-MB doped FLG.

The total change in the work function of FLG results from changes in the Fermi energy level relative to the graphene band positions as a result of electron transfer and from changes in vacuum level resulting from surface dipole formation.[27] A comparison between the shifts of the Fermi level, approximated from the binding energy of the fitted sp^2 C 1s peak in the XPS and the shifts in the work function obtained from PESA is shown in **Figure 4B and 4C**. For both $FeCl_3$

intercalation and the hybrid $FeCl_3$-MB doped FLG (**Figure 4B**), there are differences between the work-function shift and the Fermi level shift that indicate significant surface-dipole contributions to the total work function in both cases. However, in the case of Br_2-intercalated sample and hybrid Br_2-MB shown in **Figure 4C**, the shifts in the work function essentially equate with the shift in the Fermi energy level, and a considerable difference only emerges once the surface dopants are applied (hybrid Br_2-MB), indicating that the additional shift comes from vacuum-level shifts due to the formation of surface dipoles. The presence of a vacuum-level shift contribution in the case of the $FeCl_3$-intercalated sample, as contrasted to its absence in the case of the Br_2-intercalated sample, may be explained by the fact the surface dipole dominates the changes in work function at large carrier density due to the linear dependence of such a contribution on the carrier density involved in the charge transfer, whereas the Fermi-level shift contribution has a square root dependence on the carrier density.[27] Thus, the larger increase in the carrier density for $FeCl_3$ intercalation as compared to Br_2 intercalation as shown in **Figure 3B**, may lead to formation of a considerable molecular dipole buried in the bulk of FLG. For both hybrid-doped FLG samples it appears that the additional shifts in the work function seen on treating with surface doping are dominated by vacuum-level shifts, which explains the large changes in the work function as compared to the changes in the sheet carrier density.

Stability of hybrid-doped FLG

One of the key advantages of combining the intercalation doping approach with the surface molecular doping approach is the ability to enhance the stability of the doped FLG by taking advantage of the demonstrated air stability of the former. Bulk doping of FLG by intercalation leads to effective encapsulation of the intercalant molecules in between the graphene sheets from the surrounding environment.[40] Figure S6 shows the air stability of FLG intercalated with $FeCl_3$

and FLG surface doped with MB by measuring their sheet resistance. $FeCl_3$ intercalated FLG shows high stability in ambient air where the sheet resistance increases by ~ 25 Ω/□ over 7 days. However, FLG surface doped with MB shows an increase of the sheet resistance by ~ 150 Ω/□ over the same period, which is not surprising since dopant molecules are exposed on the surface of FLG. Overall, we expect that hybrid-doping approach will show higher stability in air than surface doping alone, since the low-resistance channels through the bulk (intercalation-doped FLG) will remain available in contrast to the increased resistance of the surface. We have further evaluated the dopant stability by measuring the hybrid doped FLG (Hybrid $FeCl_3$-MB) after ~ 230 days showing an increase the sheet resistance from 110 Ω/□ to 190 Ω/□. This demonstrates a very high stability of the hybrid-doping approach as a favorable route to dope graphene for industrial applications, and should be easily improved with device encapsulation and product packaging.

Conclusion

In conclusion, a versatile and stable hybrid-doping strategy for CVD-grown FLG is demonstrated, enabling efficient doping of all the graphene layers in FLG through a combination of molecular surface dopants and bulk intercalation with small molecules. The variation of the chemical composition of hybrid-doped FLG with depth reveals the existence of intercalants in the bulk of the films, which dope the interior graphene layers. The surface dopants, on the other hand, are shown to be primarily present on the exposed surfaces of FLG. It was demonstrated that the two doping modalities (intercalation and surface) work together synergistically and positively to tune the electrical transport and electronic properties of FLG. Further p-doping was observed upon surface doping of intercalated FLG, but the intercalation process is predominantly

responsible for the enhancement of the electrical conductivity, whereas surface doping helps effectively increase the work function of intercalated FLG through the formation of surface dipoles, with moderate additional increases of free-carrier density. This work demonstrates the unique platform provided by large-scale CVD grown FLG that allows for the hybrid doping strategy presented herein, which can both efficiently dope FLG with great versatility and tunability of its electrical and electronic properties.

Associated Content:

Supporting information: Additional information on the properties of as-prepared Few layers graphene, Angle resolved XPS on only intercalated FLG, Chemical States of the dopants, PESA spectra and Air stability data.

Acknowledgments

The authors acknowledge Dr. Marcel Said for the early discussion of the hybrid doping approach, Dr. Yadong Zhang for synthesis of the Mo dopant, and Mrs. Lubna Jamshaid for her logistical support. This work was supported by King Abdullah University of Science and Technology (KAUST), and Department of the Navy, Office of Naval Research Award No. N00014-14-1-0126.

References

(1) Schwierz, F. Graphene Transistors. *Nat. Nanotechnol.* **2010**, *5* (July), 487.

(2) Avouris, P. Graphene: Electronic and Photonic Properties and Devices. *Nano Lett.* **2010**, *10* (11), 4285–4294.

(3) Hong, A. J.; Song, E. B.; Yu, H. S.; Allen, M. J.; Kim, J.; Fowler, J. D.; Wassei, J. K.; Park, Y.; Wang, Y.; Zou, J.; Kaner, R. B.; Weiller, B. H.; Wang, K. L. Graphene Flash Memory. *ACS Nano* **2011**, *5* (10), 7812–7817.

(4) Bae, S.; Kim, H.; Lee, Y.; Xu, X.; Park, J.-S.; Zheng, Y.; Balakrishnan, J.; Lei, T.; Ri Kim, H.; Song, Y. Il; Kim, Y.-J.; Kim, K. S.; Özyilmaz, B.; Ahn, J.-H.; Hong, B. H.; Iijima, S. Roll-to-Roll Production of 30-Inch Graphene Films for Transparent Electrodes. *Nat. Nanotechnol.* **2010**, *5* (8), 574–578.

(5) Park, H.; Brown, P. R.; Bulović, V.; Kong, J. Graphene as Transparent Conducting Electrodes in Organic Photovoltaics: Studies in Graphene Morphology, Hole Transporting Layers, and Counter Electrodes. *Nano Lett.* **2012**, *12* (1), 133–140.

(6) Geim, A. K.; Novoselov, K. S. The Rise of Graphene. *Nat. Mater.* **2007**, *6* (3), 183–191.

(7) Bonaccorso, F.; Sun, Z.; Hasan, T.; Ferrari, A. C. Graphene Photonics and Optoelectronics. *Nat. Photonics* **2010**, *4* (9), 611–622.

(8) Lee, C.; Wei, X.; Kysar, J. W.; Hone, J. Measurement of the Elastic Properties and Intrensic Strength of Monolayer Graphene. Science. **2008**, 321(5887), *385*-388.

(9) Wallace, P. R. The Band Theory of Graphite. *Phys. Rev.* **1947**, *71* (9), 622–634.

(10) Novoselov, K. S.; Geim, a K.; Morozov, S. V; Jiang, D.; Zhang, Y.; Dubonos, S. V; Grigorieva, I. V; Firsov, A. A. Electric Field Effect in Atomically Thin Carbon Films. *Science.* **2004**, *306* (5696), 666–669.

(11) Du, X.; Skachko, I.; Barker, A.; Andrei, E. Y. Approaching Ballistic Transport in Suspended Graphene. *Nat. Nanotechnol.* **2008**, *3* (8), 491–495.

(12) Morozov, S. V.; Novoselov, K. S.; Katsnelson, M. I.; Schedin, F.; Elias, D. C.; Jaszczak, J. A.; Geim, A. K. Giant Intrinsic Carrier Mobilities in Graphene and Its Bilayer. *Phys. Rev. Lett.* **2008**, *100* (1), 16602.

(13) Nair, R. R.; Blake, P.; Grigorenko, A. N.; Novoselov, K. S.; Booth, T. J.; Stauber, T.; Peres, N. M. R.; Geim, A. K. Fine Structure Constant Defines Visual Transparency of Graphene. *Science.* **2008**, *320* (5881), 1308–1308.

(14) Novoselov, K. S.; Geim, A. K.; Morozov, S. V; Jiang, D.; Katsnelson, M. I.; Grigorieva, I. V; Dubonos, S. V; Firsov, A. A. Two-Dimensional Gas of Massless Dirac Fermions in Graphene. *Nature* **2005**, *438* (7065), 197–200.

(15) Adam, S.; Hwang, E. H.; Galitski, V. M.; Das Sarma, S. A Self-Consistent Theory for Graphene Transport. *Proc. Natl. Acad. Sci. U. S. A.* **2007**, *104* (47), 18392–18397.

(16) Tan, Y. W.; Zhang, Y.; Bolotin, K.; Zhao, Y.; Adam, S.; Hwang, E. H.; Das Sarma, S.; Stormer, H. L.; Kim, P. Measurement of Scattering Rate and Minimum Conductivity in Graphene. *Phys. Rev. Lett.* **2007**, *99* (24), 10–13.

(17) Gierz, I.; Riedl, C.; Starke, U.; Ast, C. R.; Kern, K. Atomic Hole Doping of Graphene. *Nano Lett.* **2008**, *8* (12), 4603–4607.

(18) Sreeprasad, T. S.; Berry, V. How Do the Electrical Properties of Graphene Change with Its Functionalization? *Small* **2012**, No. 3, 341–350.

(19) Mattevi, C.; Kim, H.; Chhowalla, M. A Review of Chemical Vapour Deposition of Graphene on Copper. *J. Mater. Chem.* **2011**, *21* (10), 3324.

(20) Jauregui, L. A.; Cao, H.; Wu, W.; Yu, Q.; Chen, Y. P. Electronic Properties of Grains and Grain Boundaries in Graphene Grown by Chemical Vapor Deposition. *Solid State Commun.* **2011**, *151* (16), 1100–1104.

(21) Kumari, A.; Prasad, N.; Bhatnagar, P. K.; Mathur, P. C.; Yadav, A. K.; Tomy, C. V.; Bhatia, C. S. Electrical Transport Properties of Polycrystalline CVD Graphene on SiO2/Si Substrate. *Diamond Relat. Mater.* **2014**, *45*, 28–33.

(22) Du, J.; Pei, S.; Ma, L.; Cheng, H. 25th Anniversary Article: Carbon Nanotube-and Graphene-Based Transparent Conductive Films for Optoelectronic Devices. *Adv. Mater. (Weinheim, Ger.)* **2014**, *26* (13), 1958–1991.

(23) Chen, W.; Chen, S.; Qi, D. C.; Gao, X. Y.; Wee, A. T. S.; Dong, C. Q.; Xing, Y. G.; Wee, A. T. S. Surface Transfer P-Type Doping of Epitaxial Graphene. *J. Am. Chem. Soc.* **2007**, *129* (34), 10418–10422.

(24) Shin, H.-J.; Choi, W. M.; Choi, D.; Han, G. H.; Yoon, S.-M.; Park, H.-K.; Kim, S.-W.; Jin, Y. W.; Lee, S. Y.; Kim, J. M.; Choi, J.-Y.; Lee, Y. H. Control of Electronic Structure of Graphene by Various Dopants and Their Effects on a Nanogenerator. *J. Am. Chem. Soc.* **2010**, *132* (44), 15603–15609.

(25) Christodoulou, C.; Giannakopoulos, a.; Nardi, M. V.; Ligorio, G.; Oehzelt, M.; Chen, L.; Pasquali, L.; Timpel, M.; Giglia, A.; Nannarone, S.; Norman, P.; Linares, M.; Parvez, K.; Müllen, K.; Beljonne, D.; Koch, N. Tuning the Work Function of Graphene-on-Quartz with a High Weight Molecular Acceptor. *J. Phys. Chem. C* **2014**, *118* (9), 4784–4790.

(26) Kim, Y.; Ryu, J.; Park, M.; Kim, E. S.; Yoo, J. M.; Park, J.; Kang, J. H.; Hong, B. H. Vapor-Phase Molecular Doping of Graphene for High-Performance Transparent Electrodes. *ACS Nano* **2014**, *8* (1), 868–874.

(27) Paniagua, S. A.; Baltazar, J.; Sojoudi, H.; Mohapatra, S. K.; Zhang, S.; Henderson, C. L.; Graham, S.; Barlow, S.; Marder, S. R. Production of Heavily N- and P-Doped CVD Graphene with Solution-Processed Redox-Active Metal–organic Species. *Mater. Horiz.* **2014**, *1* (1), 111–115.

(28) Bult, J. B.; Crisp, R.; Perkins, C. L.; Blackburn, J. L. Role of Dopants in Long-Range Charge Carrier Transport for P-Type and N-Type Graphene Transparent Conducting Thin Films. *ACS Nano* **2013**, *7* (8), 7251–7261.

(29) Chen, L.; Wang, L.; Shuai, Z.; Beljonne, D. Energy Level Alignment and Charge Carrier Mobility in

Noncovalently Functionalized Graphene. *J. Phys. Chem. Lett.* **2013**, *4* (13), 2158–2165.

(30) Hsu, C. L.; Lin, C. Te; Huang, J. H.; Chu, C. W.; Wei, K. H.; Li, L. J. Layer-by-Layer graphene/TCNQ Stacked Films as Conducting Anodes for Organic Solar Cells. *ACS Nano* **2012**, *6* (6), 5031–5039.

(31) Günes, F.; Shin, H.; Biswas, C.; Han, G. H.; Kim, E. S.; Chae, S. J.; Choi, J.-Y.; Lee, Y. H. Layer-by-Layer Doping of Few-Layer Graphene Film. *ACS Nano* **2010**, *4* (8), 4595–4600.

(32) Kasry, A.; Kuroda, M. a.; Martyna, G. J.; Tulevski, G. S.; Bol, A. a. Chemical Doping of Large-Area Stacked Graphene Films for Use as Transparent, Conducting Electrodes. *ACS Nano* **2010**, *4* (7), 3839–3844.

(33) Wang, Y.; Tong, S. W.; Xu, X. F.; Ozyilmaz, B.; Loh, K. P. Interface Engineering of Layer-by-Layer Stacked Graphene Anodes for High-Performance Organic Solar Cells. *Adv. Mater. (Weinheim, Ger.)* **2011**, *23* (13), 1514–1518.

(34) Fu, X. W.; Liao, Z. M.; Zhou, J. X.; Zhou, Y. B.; Wu, H. C.; Zhang, R.; Jing, G.; Xu, J.; Wu, X.; Guo, W.; Yu, D. Strain Dependent Resistance in Chemical Vapor Deposition Grown Graphene. *Appl. Phys. Lett.* **2011**, *99* (2011), 3–5.

(35) Li, X.; Zhu, Y.; Cai, W.; Borysiak, M.; Han, B.; Chen, D.; Piner, R. D.; Colombo, L.; Ruoff, R. S. Transfer of Large-Area Graphene Films for High-Performance Transparent Conductive Electrodes. *Nano Lett.* **2009**, *9* (12), 4359–4363.

(36) Kim, K. S.; Zhao, Y.; Jang, H.; Lee, S. Y.; Kim, J. M.; Kim, K. S.; Ahn, J.-H.; Kim, P.; Choi, J.-Y.; Hong, B. H. Large-Scale Pattern Growth of Graphene Films for Stretchable Transparent Electrodes. *Nature* **2009**, *457* (7230), 706–710.

(37) Dresselhaus, M. S.; Dresselhaus, G. Intercalation Compounds of Graphite. *Adv. Phys.* **2002**, *51* (1), 1–186.

(38) Bao, W.; Wan, J.; Han, X.; Cai, X.; Zhu, H.; Kim, D.; Ma, D.; Xu, Y.; Munday, J. N.; Drew, H. D.; Fuhrer, M. S.; Hu, L. Approaching the Limits of Transparency and Conductivity in Graphitic Materials through Lithium Intercalation. *Nat. Commun.* **2014**, *5*, 4224.

(39) Khrapach, I.; Withers, F.; Bointon, T. H.; Polyushkin, D. K.; Barnes, W. L.; Russo, S.; Craciun, M. F. Novel Highly Conductive and Transparent Graphene-Based Conductors. *Adv. Mater.* (Weinheim, Ger.) **2012**, *24* (21), 2844–2849.

(40) Mansour, A. E.; Dey, S.; Amassian, A.; Tanielian, M. H. Bromination of Graphene: A New Route to Making High Performance Transparent Conducting Electrodes with Low Optical Losses. *ACS Appl. Mater. Interfaces* **2015**, *7* (32), 17692–17699.

(41) Wehenkel, D. J.; Bointon, T. H.; Booth, T.; Bøggild, P.; Craciun, M. F.; Russo, S. Unforeseen High Temperature and Humidity Stability of $FeCl_3$ Intercalated Few Layer Graphene. *Sci. Rep.* **2015**, *5*, 7609.

(42) Zhao, W.; Tan, P. H.; Liu, J.; Ferrari, A. C. Intercalation of Few-Layer Graphite Flakes with $FeCl_3$: Raman Determination of Fermi Level, Layer by Layer Decoupling, and Stability. *J. Am. Chem. Soc.* **2011**, *133* (15), 5941–5946.

(43) Mansour, A. E.; Said, M. M.; Dey, S.; Hu, H.; Zhang, S.; Munir, R.; Zhang, Y.; Moudgil, K.; Barlow, S.; Marder, S. R.; Amassian, A. Facile Doping and Work-Function Modification of Few-Layer Graphene Using Molecular Oxidants and Reductants. *Adv. Funct. Mater.* **2017**, 27(7), 1602004.

(44) Connelly, N. G.; Geiger, W. E. Chemical Redox Agents for Organometallic Chemistry. *Chem. Rev.* **1996**, *96* (2), 877–910.

(45) Mohapatra, S. K.; Zhang, Y.; Sandhu, B.; Fonari, M. S.; Timofeeva, T. V.; Marder, S. R.; Barlow, S. Synthesis, Characterization, and Crystal Structures of Molybdenum Complexes of Unsymmetrical Electron-Poor Dithiolene Ligands. *Polyhedron.* **2016**, 116, 88-95.

(46) Bointon, T. H.; Jones, G. F.; De Sanctis, A.; Hill-Pearce, R.; Craciun, M. F.; Russo, S. Large-Area Functionalized CVD Graphene for Work Function Matched Transparent Electrodes. *Sci. Rep.* **2015**, *5*, 16464.

(47) Zhan, D.; Sun, L.; Ni, Z. H.; Liu, L.; Fan, X. F.; Wang, Y.; Yu, T.; Lam, Y. M.; Huang, W.; Shen, Z. X. $FeCl_3$-Based Few-Layer Graphene Intercalation Compounds: Single Linear Dispersion Electronic Band Structure and Strong Charge Transfer Doping. *Adv. Funct. Mater.* **2010**, *20* (20), 3504–3509.

(48) Yan, Z.; Zhuxia, Z.; Tianbao, L.; Xuguang, L.; Bingshe, X. XPS and XRD Study of $FeCl_3$–graphite Intercalation Compounds Prepared by Arc Discharge in Aqueous Solution. *Spectrochim. Acta, Part A* **2008**, *70* (5), 1060–1064.

(49) Usha, N.; Viswanathan, B.; Murthy, V. R. K.; Sobhanadri, J. X-Ray Photoelectron Spectroscopic Study of Some Pure Stages of Graphite Ferric Chloride Intercalation Compounds. *Spectrochim. Acta, Part A* **1997**, *53* (11), 1761–1765.

(50) Ferrari, A. C. Raman Spectroscopy of Graphene and Graphite: Disorder, Electron–phonon Coupling, Doping and Nonadiabatic Effects. *Solid State Commun.* **2007**, *143* (1–2), 47–57.

(51) Faugeras, C.; Nerrière, A.; Potemski, M.; Mahmood, A.; Dujardin, E.; Berger, C.; de Heer, W. A. Few-Layer Graphene on SiC, Pyrolitic Graphite, and Graphene: A Raman Scattering Study. *Appl. Phys. Lett.* **2008**, *92* (1), 11914.

(52) Song, J. J.; Chung, D. D. L.; Eklund, P. C.; Dresselhaus, M. S. Raman Scattering in Graphite Intercalation Compounds. *Solid State Commun.* **1976**, *20* (12), 1111–1115.

(53) Das, A.; Pisana, S.; Chakraborty, B.; Piscanec, S.; Saha, S. K.; Waghmare, U. V; Novoselov, K. S.; Krishnamurthy, H. R.; Geim, A. K.; Ferrari, A. C.; Sood, A. K. Monitoring Dopants by Raman Scattering in an Electrochemically Top-Gated Graphene Transistor. *Nat. Nanotechnol.* **2008**, *3* (4), 210–215.

TOC Figure

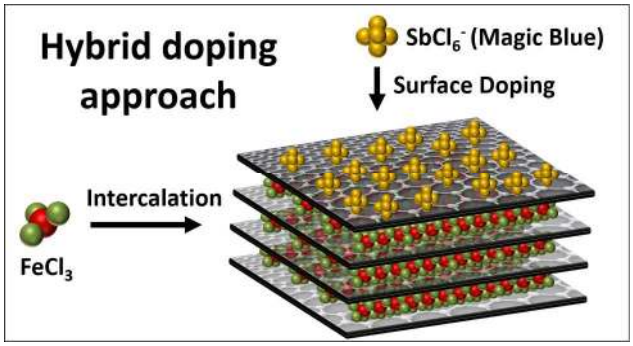

For table of content only.